

Plant-Based Mycetoma Inhibitors Targeting the 50S Ribosomal Protein of *Nocardia brasiliensis*: In Silico Approach

Sandra Jose,^[a] Manjunathan Jagadeesan,^[b] Meenambiga Setti Sudharsan,^[a] Pasiyappazham Ramasamy,^[c, d] Shyamala Gowri,^[e] Muthu Thiruvengadam,^{*,[f]} Sowmya Hari,^{*,[a]} and Baskar Venkidasamy^[g]

Mycetoma is a subcutaneous, potentially serious, and devastating chronic disease caused by aerobic actinomycetes (actinomycetoma) or fungi (eumycetoma). *Nocardia* species causes pulmonary, cutaneous, and subcutaneous human diseases, especially mycetoma, and the most commonly isolated species include *Nocardia brasiliensis*. Drug development to combat this illness is still in progress, although it is highly neglected, and most importantly, no vaccination is available for the disease. We used an in silico approach to screen a library of 1034 phytochemicals to obtain the most potent compound for the treatment

of mycetoma. Parviflorone F is known for its antimalarial activity and enhanced protein stability upon binding, indicating efficient inhibition of the protein. The positional fluctuations of parviflorone F located inside the binding site were explored and the effect of binding on the dynamic stability of the protein was assessed. This study explored drug-like phytochemicals with good inhibitory effects against the 50S ribosomal unit of *N. brasiliensis*, indicating that they can be used for the treatment of mycetoma after confirmation in in vitro and in vivo studies.

1. Introduction

Mycetoma is a chronic, occasionally lethal, skin infection caused by fungi (Eumycetoma) or aerobic actinomycete bacteria (actinomycetoma). Actinomycetoma is currently treated with antibi-

otics, either alone or in combination, based on its location, intensity, and dissemination.^[1] Actinomycetoma and eumycetoma have different global incidences depending on the country, although they are most prevalent between 30°N and 15°S. India, Sudan, Venezuela, and Mexico had the highest numbers of mycetoma cases. The highest prevalence of eumycetoma (up to 70%) was reported in Sudan.^[2] Patients typically receive a medical cure if they receive appropriate care. Treatment of eumycetoma involves surgical excision and antifungal treatment. However, medical treatment is more challenging because of the possibility of persistent, progressive lesions that almost always require excision due to the course and location of the disease. Nonetheless, prolonged behavior is necessary for both types of mycetoma.^[3] Soil-found fungi, called eumycetes and actinomycetes, are believed to cause infections when repeatedly injected traumatically into the skin.^[4,5] Clinically, there is a firm, usually painless, enlargement of the lower limbs, with several sinus tracts that discharge grains and serosanguinous purulent fluid. These grains are colonies of pathogenic organisms.^[6]

The causative organism of mycetoma largely dictates its course of treatment; actinomycetomas respond more strongly to antimicrobial chemotherapy than eumycetomas. Ninety percent of actinomycetomas are believed to be curable with medication even in cases of significant bone involvement. Surgery is a common treatment for mild eumycetoma.^[7] If the eumycetomas are too large to be completely removed, debulking procedures or excisions are required. Local infection recurrence is common following the surgical excision of both actinomycetomas and eumycetomas.^[8] Dapsone and sulfonamides are the best medications for the treatment of mycetomas caused by *N. brasiliensis*. Currently, the most successful treatment course is a combination of trimethoprim and sulfamethoxazole. Furthermore, amikacin appears to be effective when used alone or in combination with trimethoprim and sulfamethoxazole. Other medications used to

[a] S. Jose, M. S. Sudharsan, S. Hari

Department of Bioengineering, School of Engineering, Vels Institute of Science Technology and Advanced Studies, Chennai 600117, India
E-mail: sowmya.se@velsuniv.ac.in

[b] M. Jagadeesan

Department of Biotechnology, School of Life Sciences, Vels Institute of Science Technology and Advanced Studies, Chennai 600117, India

[c] P. Ramasamy

Department of Prosthodontics and Implantology, Saveetha Dental College & Hospitals, Saveetha Institute of Medical and Technical Sciences, Saveetha University, Chennai 600077, India

[d] P. Ramasamy

Polymer Research Laboratory (PR Lab), Centre for Marine Research and Conservation, Saveetha Dental College & Hospitals, Saveetha Institute of Medical and Technical Sciences, Saveetha University, Chennai 600077, India

[e] S. Gowri

Department of Botany, Pachaiyappas College, Chennai 600030, India

[f] M. Thiruvengadam

Department of Applied Bioscience, College of Life and Environmental Science, Konkuk University, Seoul 05029, Republic of Korea
E-mail: muthu@konkuk.ac.kr

[g] B. Venkidasamy

Department of Oral & Maxillofacial Surgery, Saveetha Dental College and Hospitals, Saveetha Institute of Medical and Technical Sciences, Saveetha University, Chennai 600077, India

Supporting information for this article is available on the WWW under <https://doi.org/10.1002/slct.202404337>

© 2025 The Author(s). ChemistrySelect published by Wiley-VCH GmbH. This is an open access article under the terms of the [Creative Commons Attribution License](#), which permits use, distribution and reproduction in any medium, provided the original work is properly cited.

treat mycetomas caused by *N. brasiliensis* include streptomycin sulfate, rifampin, and isoniazid.^[9] Because of the ability of *N. brasiliensis* to produce beta-lactamase, beta-lactam antibiotics are usually ineffective. However, this resistance may be overcome by supplementing the antibiotic with clavulanic acid. Combinations of two or more medications yield better results than single medications.^[10]

As *N. brasiliensis* mycetomas require long-term treatment, it is important to thoroughly assess the potential toxicity of aminoglycosides before initiating the treatment. Having realized how bad the illness was, we decided to concentrate on mycetoma and identify effective natural ingredients to develop drugs to treat this condition. Several studies have demonstrated that 50S ribosomal protein L28, which is produced by the *rpmB* gene, may be a target for inhibiting the bacterial *N. brasiliensis* protein translation machinery.^[11–14] It is a member of the L28 family of bacterial ribosomal proteins (RPs). According to the results of the current study, the 50S ribosomal protein L28 carries out important molecular functions such as rRNA binding. 50S ribosomal protein L28 participates in two biological processes: translation and ribosomal large subunit assembly. Consequently, L28 was selected as the target of this study because its blockage may lower the activity of *N. brasiliensis*.^[15]

Many different ailments have been treated using natural products (NP). The structural complexity, chemical diversity, and biological specialization that distinguish NPs from manufactured molecules are the result of evolution.^[16] In the process of developing new drugs, NP scaffolds are considered essential; from 1981 to 2010, over 64% of authorized medications were either inspired by or derived from NPs. Phase III clinical studies of 31 additional compounds are currently underway, or have been completed since 2008. Twenty-five novel NP-derived drugs have been approved since 2008. Several NP databases have been constructed to support in silico drug development studies. It is a common practice to retrieve chemicals for different investigations from the South African Natural Compound Database (SANCDB) and traditional Chinese plants and medicines.^[17] To investigate the possibility of using drug-like phytomolecules from SANCDB against 50S ribosomal protein L28 to prevent mycetoma infection, we employed extensive in silico studies. Mycetoma is a chronic tropical disease that is caused by fungi and bacteria. The current treatment options are limited and ineffective. Therefore, plant-based inhibitors may be safer and more effective alternatives. Several plant-derived substances exhibit intriguing antibacterial properties. This study can assist in identifying new bioactive compounds for the development of tailored mycetoma inhibitors. However, synthetic medications are expensive. Exploring plant-based inhibitors could lead to cost-effective treatment solutions, particularly in the affected regions of Africa, South America, and Asia.

2. Material and Methods

2.1. Sequence Retrieval and Function Analysis

The protein sequence of the 50S ribosomal protein L28 was obtained from NCBI which consists of protein sequences and

structures. Among various other bacterial proteins, this protein mainly functions in translation and rRNA binding. A biological database and online resource with multiple sources of data on known and projected protein-protein interactions is called the search tool for the retrieval of interacting genes/proteins (STRING).^[18]

2.2. Physicochemical Characterization

The retrieved sequences were analyzed using the in silico ExPASy-ProtParam tool. This tool helps to calculate molecular weight, theoretical pI, atomic composition, amino acid composition, extinction coefficient, estimated half-life, instability index, aliphatic index, and grand average of hydrophilicity (GRAVY), among other physicochemical characteristics of the primary protein structure. This method is mostly used to determine the stability of sequenced proteins.

2.3. Homology Modelling of 50s Ribosomal Unit of *N. brasiliensis*

Protein secondary structure prediction has been greatly improved by consensus prediction based on multiple alignments. The primary structure was initially identified using SOPMA. SWISS-MODEL was used to model the homology of the 50S ribosomal unit of *N. brasiliensis*.^[19]

2.4. Refinement and Structure Validation

The modelled protein was refined using an updated version of GalaxyRefine and intricate refinement was performed using stronger harmonic restraints validated by analyzing the Ramachandran plot. The plot was predicted using the PROCHECK database for the refined protein structure generated using Galaxy Refine 2.0, to determine the quantity of residues in both permitted and prohibited areas. The PDB file was downloaded, and MolProbity, clash score, poor rotamers, and ramachandran favored regions of the protein structure were calculated using the SWISS structural assessment tool, which is an extensively used system for protein structure validation.^[20] The modelled protein was evaluated based on web-based tools such as VERIFY3D, ERRAT, and PROVE (<https://saves.mbi.ucla.edu/>), and the standard Voronoi method was applied to compute the fractional accessible surface area, fractional residue volume, stereo/packing quality index, and 3D profile quality index. (<http://vadar.wishartlab.com/>).

2.5. Ligand Preparation

SANCDB, a South African natural compound database, is an NP database consisting of 1034 compounds.^[21] The retrieved SDF files were optimized using the UCSF Chimera. These ligands were prepared and saved in the pdbqt format. PubChem

was used to obtain the data. The SDF format of the control (amikacin) structure and drug was optimized and prepared for docking using the techniques used for the ligands from SANCDB.

2.6. ADMET Screening of the Database

SWISS-ADME was used to examine and filter molecules based on their adsorption, distribution, metabolism, and excretion using smiles obtained from PubChem. The filtered compounds were studied for toxicity using PreADMET. Finally, drug-likeness of the filtered compounds was investigated. Compounds were strictly screened based on Lipinski et al.,^[22] Ghose et al.,^[23] Veber et al.,^[24] Egan et al.,^[25] and Muegge's rules.^[26] Compounds that did not satisfy this set of rules were excluded from further analysis.^[27]

2.7. Molecular Docking-Based Virtual Screening and Analysis

Virtual screening (VS) could also be a computational technique utilized in drug discovery to identify libraries of small molecules, such that structures presumably bind to a drug target, typically a protein receptor or enzyme. The VS of all 229 filtered compounds was determined using AutoDockVina software. A score was used to calculate the binding energies between the protein and the ligand.^[28] AutoDockVina was significantly better than AutoDock 4.^[29] The best-scoring compounds were analyzed using Discovery studio 3.5 and PyMOL 2.

2.8. Molecular Dynamics Simulations

Molecular dynamics (MD) simulations are regarded as an authoritative step in computational research on drug discovery at the atomic level. The internal motions of proteins can reveal many hidden biological functions as well as their profound dynamic mechanisms. It shows dynamic changes over time, allowing us to determine whether the protein–ligand complex is stable.^[30] For the 100-ns timeframe MD simulations of ligand-free and ligand-bound forms, the compound with the highest affinity toward the protein target was found. To perform the MD simulations, we used the GROMACS 2018.1 software. For all atoms, CHARMM 27 force fields were used to parameterize the protein–ligand complexes. A simple point charge (SPC/E) was used as the solvent, and the charge was adjusted by adding Na⁺ or Cl[−] ions to mimic the physiological system environment. The energy of these systems was then reduced using the steepest descent algorithm with a tolerance of 1000 kJ/mol/nm. The complexes were then counterpoised for 0.1 ns using NVT and NPT ensembles with position restraint on the protein molecules. The particle mesh Ewald (PME) was created to deal with long-range Coulomb interactions using a 0.12 nm Fourier grid spacing. The Lennard–Jones potential with a cut-off distance of 1 nm was used to calibrate short-range van der Waals interactions. To assess stability for 100 ns, MD simulations were performed without any constraints

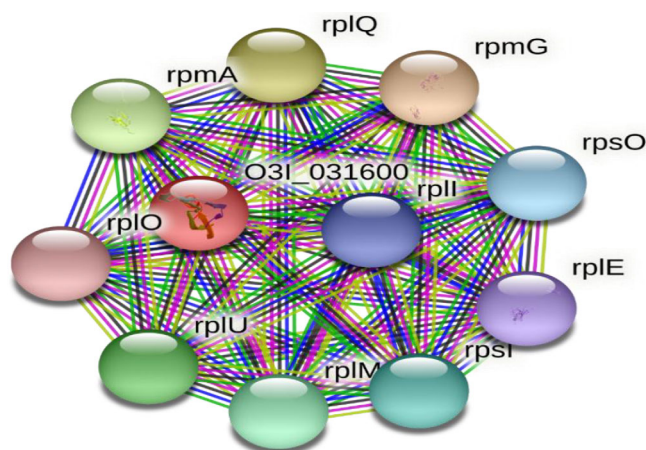


Figure 1. STRING protein-protein interaction network consisting of both functional and physical interactions.

on the protein molecules or ligands. Finally, some of the GRO-MACS modules were used to analyze the MD trajectories, such as the gmxrms, gmxrmsf, and gmx gyrate.

3. Results

3.1. Sequence Retrieval and Function Analysis

50S subunit ribosomal protein L28 of *N. brasiliensis* was selected as the target protein of interest. The NCBI Reference sequence was WP_08,187,8274.1. The primary sequence of the protein was retrieved from NCBI, and the sequences in the FASTA format (https://www.ncbi.nlm.nih.gov/protein/WP_081878274.1?report=fasta) were downloaded for further analysis. Specific protein names and source organisms were provided as inputs to STRING, and the physical and functional interactions were studied. The results of the primary analysis are shown in Figure 1.

During primary expansion, the major nodes that interacted with query O3I_03,1600 were rplE, rplI, rplM, rplO, rplQ, rplU, rpmA, rpmG, rpsI, and rpsO. Major functional analyses are presented in Table 1. Primary function analysis confirmed the active participation of this protein along with other proteins that are primarily involved in translation and post-translational events. Hence, 50S subunit ribosomal protein L28 is a potential target for inhibiting translation.

3.2. Physicochemical Characterization

3.2.1. Calculations were Made to Determine Physicochemical Properties

Protein instability and aliphatic indices confirmed the validity of this structure. The solidity of the structure was confirmed using the aliphatic and protein instability indices. Alanine, valine, isoleucine, and leucine have significantly high-volume occupations (51.35 aliphatic index), which may contribute to the thermostability of the protein. The revised and energetically reduced

Table 1. Interaction analysis between several nodes that are primarily linked to the selected protein and their functions is represented through annotation.

Interacting Protein	Annotation
rplE	One of the proteins that binds and most likely mediates the attachment of the 5S RNA into the big ribosomal subunit, where it is a component of the central protuberance, is the 50S ribosomal protein L5. It makes contact with protein S13 of the 30S subunit (bridge B1b) in the 70S ribosome, linking the two subunits; this bridge is involved in subunit migration. It makes contact with the P site tRNA; the 5S rRNA and a few of its related proteins may aid in stabilizing the placement of tRNAs attached to ribosomes.
rplI	50S ribosomal protein (RP) L9; joins with 23S rRNA
rplM	50S RP L13; important during the early stages of 50S assembly
rplO	50S RP L15; binds to the 23S rRNA
rplQ	COG0203 RP L17
rplU	50S RP L21; this protein binds to 23S rRNA in the presence of protein L20
rpmA	COG0211 RP L27; bL27 family
rpmG	COG0267 RP L33; belongs to the bacterial protein bL33 family
rpsI	COG0103 RP S9; uS9 family
rpsO	30S RP S15; forms abridge B4 with the 23S rRNA

Table 2. The values for the physicochemical characteristics of the protein structure were calculated using the ProtParam tool from the Swiss expasy.

Property	Determined Value
Number of amino acids	74
Molecular weight	8158.53
Theoretical pI	11.61
Total number of negatively charged residues	2
Total number of positively charged residues	18
Ext. coefficient	1740 M ⁻¹ cm ⁻¹
Estimated half-life	30 h (mammalian reticulocytes, in vitro) >20 h (yeast, in vivo) >10 h (<i>Escherichia coli</i> , in vivo)
Instability index	65.88
Aliphatic index	51.35
Grand average of hydropathicity	−0.769

structures had an instability index greater than 40. A slightly negative GRAVY score (−0.769), which represents the ratio between the total hydrophathy values and the number of residues in the given sequence, suggests that the complex has a moderately hydrophilic character. Their physicochemical properties are listed in Table 2.

3.3. Homology Modelling

The primary structure of this protein is shown in Figure S1. Homology modelling was performed using the SWISS model with the template LSU ribosomal protein L28P, *Mycobacterium smegmatis* 70S ribosome (PDB ID: 5O61), which is 59.68 homologous. The target sequence and template structures were aligned using HHBlits; a model was built, and its quality was assessed. Figure 2 shows the template protein superimposed on its refined structure.

3.4. Structure Assessment and Refining

The modelled protein had a MolProbity Score of 1.97 and a Clash Score of, 5.31 while the structure was refined, which reduced the MolProbity score to 0.72, and the Clash score to 0.00. The Ramachandran plot was evaluated for the modelled protein before and after refinement using PROCHECK software. This increased the Ramachandran favored region to 96.2% from 94.2, maintaining the disallowed region and generously allowed region at 0 (Figure 3). QMEAN score got decreased to −2.29 to −1.52 (Figure 4). Initially, the energy of the structure was −129.17 as per determined by GalaxyRefine 2.0. After refining the structure, the total energy of the structure was reduced to −1205.69. A better quality than a typical structure at this resolution is a structure with a MolProbity score that is numerically lower than the actual crystallographic resolution. The number of poor rotamers decreased from 8.0 to 0.0 and, indicating that the structure now has better quality than before. These preliminary tests were followed by evaluation using VERIFY3D in which 79.03% of the residues had an average 3D-1D score > 0.2. In the PROVE test, the total number of buried outlier protein atoms from one model (1.7%) and ERRAT assessment (82.1429) were reported as overall quality factors. The fractional accessible surface area, fractional residue volume, stereo/packing quality index, and 3D profile quality index were calculated using the standard Voronoi procedure. The graphical representations indicated that the protein structure was stable and the quality of the modelled protein was considerably good. The values obtained for the fractional accessible surface area (ASA) with ASA values below 1 indicate the overall stability of the structure. The fractional residue volume was also lies between 1.2 and 0.8, whereas the stereo/packing quality index and 3D profile quality index were higher, as shown in Supporting Information Figure S2.

3.5. ADMET Analysis and Selection of Drug-Like Compounds

The preclinical ADME properties are vital for the development of novel drugs. All 1034 compounds were screened for their ADME properties. The 229 compounds studied followed Lipinski's, Ghose, Veber, Egan, and Muegge rules, and were selected based on their non-blood-barrier permeation properties. A strongly negative Log P value was obtained for these molecules, indicating a stronger affinity for the aqueous phase. All 229 compounds showed bioavailability of 55%. Additionally,

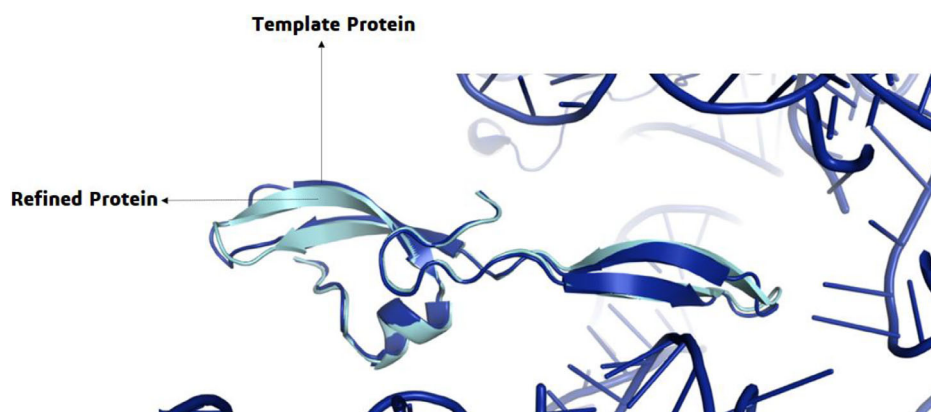
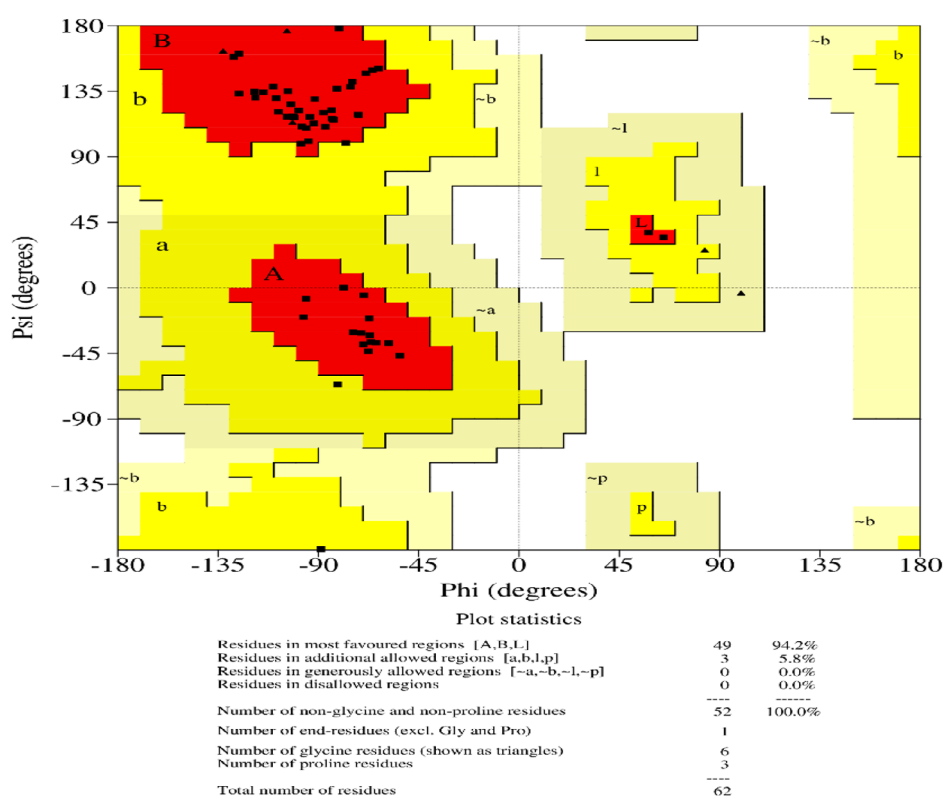


Figure 2. Structural superimposition of the template (structure of the *Mycobacterium smegmatis* 70S ribosome (PDB ID-5O61)) and refined protein using PyMol.



Based on an analysis of 118 structures of resolution of at least 2.0 Angstroms and R-factor no greater than 20%, a good quality model would be expected to have over 90% in the most favoured regions.

Figure 3. Ramachandran plot of the modelled protein-50S ribosomal unit of *N. brasiliensis*.

all compounds showed high gastrointestinal absorption. Parviflorone F was predicted to have no carcinogenic effects or eye irritation or tested positive in Ames mutagenesis. In addition, the compound showed a lower acute oral toxicity (c). All the analyses are presented in Table 3.

3.6. Molecular Docking

All 229 compounds and the control (amikacin) were docked with refined proteins using AutoDockVina. Based on the ADMET filter-

ing process, parviflorone F with a binding affinity -6.9 Kcal/mol showed better interaction when compared with compounds like tingenine B (-6.7 Kcal/mol), clonamine D (-6.6 Kcal/mol), kraussianone1 (-6.6 Kcal/mol), kraussianone4 (-6.6 Kcal/mol), kraussianone 6 (-6.6 Kcal/mol), mamegakinone (-6.6 Kcal/mol), 7-dehydroagapanthagenin (-6.6 Kcal/mol), 20-hydroxy-20-epi-tingenone (-6.5 Kcal/mol), bromotopsentin (-6.5 Kcal/mol), and valdivone B (-6.5 Kcal/mol) (Table 4). All 229 compounds showed better binding affinity scores than amikacin, which has a binding energy of only -4.6 Kcal/mol. Parviflorone F exhibits three hydrogen bonds with ASN 32, GLY 13, and GLY 11, a pi-cation

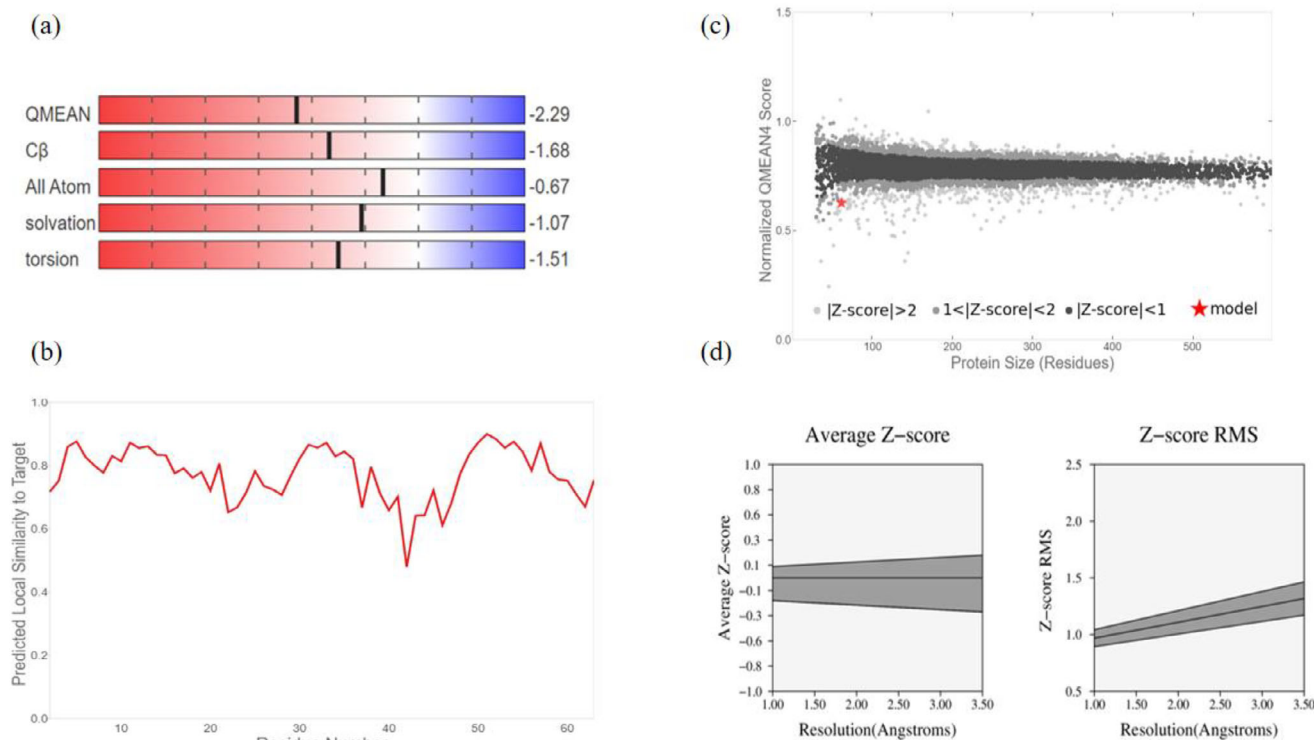


Figure 4. (a–c) The quality estimates using QMEAN. (d) Representation of buried outlier protein atoms in the form of the average Z-score and Z-score RMS.

bond with LYS 10, a Pi alkyl bond with PRO 31, a Pi-pi stacked bond with TRP 29, and four van der Waals interactions with ASN 30, PRO 12, LYS 16, and GLY 15 of the protein. The interaction diagram, in 2D, 3D with and without the complete receptor, is shown in the diagram for the best two ligands, parviflorone F and tingenine B (Figure 5).

3.7. Molecular Dynamic Simulation of the Protein–Ligand Complex

3.7.1. Conformational Stability of Native Protein and Ligand Complex

The root mean square deviation (RMSD) is among the most crucial basic characteristics for determining the stability and alignment with experimental structures.^[31] The RMSD plot suggests that binding of parviflorone F stabilizes the protein and leads to fewer structural deviations from its native conformation (Figure 6). In the case of the apo protein and protein-parviflorone F complex, the binding of parviflorone F to the protein active pocket showed low initial fluctuations until 2 ns of the MD trajectories; thereafter, it attained a high RMSD value, stably from to 2–45 ns. If we consider the dynamic behavior of parviflorone F inside the binding pocket of the protein, we can see that the dynamics of parviflorone F are more stable and fluctuate less than those of the native protein structure (Figure 6a). The orientation of parviflorone F inside the binding site was observed for five periods during the MD simulation. This leads to more dynamics in the backbone of the protein during the 100 ns MD

simulation. The root mean square fluctuations (RMSF) of the backbone atoms of the protein are shown in Figure 6b. The figure reveals that The RMSF values of parviflorone F complexed with protein were lower than those of the apo form of protein, indicating increased blocking.

3.7.2. Radius of Gyration (Rg)

Radius of gyration (Rg) is a determinant factor in the evaluation of dynamic stability.^[32] The Rg values of the proteins are shown in Figure 7.

4. Discussion

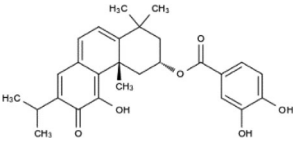
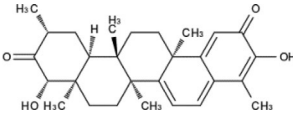
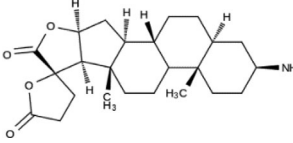
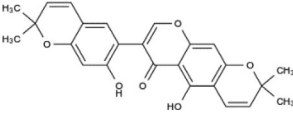
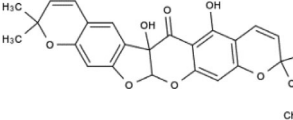
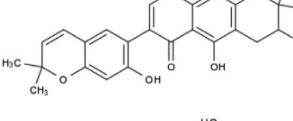
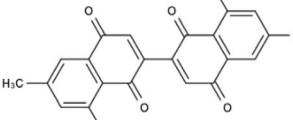
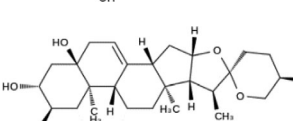
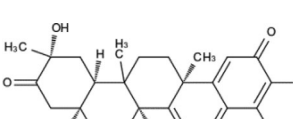
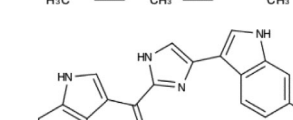
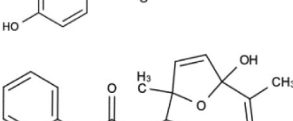
Mycetoma causative agents are found in the environment and are inoculated by splinters or other small or unnoticed damage to produce illness. It primarily affects men between the ages of 20 and 40 years who work outside (for example, farmers).^[33,34] Sudan is considered to be the world's most endemic mycetoma. Approximately 7000 people are treated for mycetoma in Khartoum, Sudan's capital, whereas actinomycetomas are more common in Mexico and Brazil, with *N. brasiliensis* being the most common causative agent.^[35] Amikacin (15 mg/kg/day) is currently the first-line therapy for actinomycetoma, with one–4–5-week cycles suggested. Amikacin has been linked to carbapenems such as imipenem or meropenem in patients resistant to TMP-SMX.^[36] Another recent study by Mohammed et al.^[37] used novel immunoinformatics approaches to discover an epitope-grounded peptide vaccine, fructose-bisphosphate aldolase of

Table 3. Compounds with the best docking scores depicted with their important characteristics and parameters.

Name Of The Compound	Parviflorone F	Tingenine B	Clonamine D	Kraussianone 1	Kraussianone 4	Kraussianone 6	Mamegakinone	7-Dehydroaga-panthagenin	20-hydroxy-20-epi-tingenone	Bromotopsentin	Valdivone B
Molecular weight	450.52	436.58	401.54	418.44	434.44	436.45	374.34	333.38	436.58	421.25	450.57
No. of heavy atoms	33	32	29	31	32	32	28	24	32	27	33
No. of aromatic heavy atoms	6	0	0	16	12	16	12	6	0	23	6
No. of rotatable bonds	4	0	0	1	0	1	1	3	0	3	5
No. of H-bond acceptors	6	4	5	6	7	7	6	6	4	3	5
No. of H-bond donors	3	2	1	2	2	3	2	2	2	4	1
MR	126.11	126.34	109.59	120.21	116.38	121.05	100.35	91.22	126.38	107.33	128.4
TPSA	104.06	74.6	78.62	89.13	94.45	109.36	108.74	71.39	74.6	97.56	72.83
Consensus Log P	4.07	4.29	3.47	4.16	3.46	3.51	2.82	0.69	4.38	3.44	3.93
ESOL class	Moderately soluble	Moderately soluble	Moderately soluble	Moderately soluble	Moderately soluble	Moderately soluble	Moderately soluble	Very soluble	Moderately soluble	Moderately soluble	Moderately soluble
Ali class	Poorly soluble	Moderately soluble	Moderately soluble	Poorly soluble	Moderately soluble	Moderately soluble	Moderately soluble	Very soluble	Moderately soluble	Moderately soluble	Moderately soluble
Silicos-IT class	Moderately soluble	Moderately soluble	Soluble	Poorly soluble	Moderately soluble	Poorly soluble	Moderately soluble	Soluble	Moderately soluble	Poorly soluble	Moderately soluble
GI absorption	High	High	High	High	High	High	High	High	High	High	High
BBB permeant	No	No	No	No	No	No	No	No	No	No	No
Pgp substrate	Yes	Yes	Yes	No	No	Yes	No	No	Yes	No	Yes
CYP1A2 inhibitor	No	No	No	No	Yes	No	Yes	No	No	Yes	No

Table 3. (Continued)											
Name Of The Compound	Parviflorone F	Tingenine B	Clonamine D	Kraussianone 1	Kraussianone 4	Kraussianone 6	Mamegakinone	7-Dehydroaga-panthagenin	20-hydroxy-20-epi-tingenone	Bromotopsentin	Valdivone B
CYP2C19 inhibitor	No	No	No	Yes	Yes	No	No	No	No	Yes	No
CYP2C9 inhibitor	Yes	Yes	No	Yes	Yes	Yes	Yes	No	Yes	No	No
CYP2D6 inhibitor	No	No	No	No	No	No	No	No	No	Yes	No
CYP3A4 inhibitor	Yes	Yes	No	No	Yes	No	Yes	No	Yes	No	Yes
Log Kp (cm/s)	−5.58	−5.65	−5.76	−5.39	−5.93	−6.16	−5.93	−8.64	−5.79	−6.04	−6.45
Lipinski #violations	0	0	0	0	0	0	0	0	0	0	0
Ghose #violations	0	0	0	0	0	0	0	0	0	0	0
Egan #violations	0	0	0	0	0	0	0	0	0	0	0
Muegge #violations	0	0	0	0	0	0	0	0	0	0	0
Bioavailability score	0.55	0.55	0.55	0.55	0.55	0.55	0.55	0.55	0.55	0.55	0.55
Synthetic accessibility	4.93	6.27	5.73	4.19	4.82	4.72	3.34	4.5	6.18	2.79	6.95
Ames mutagenesis	−	−	+	−	+	+	+	−	−	−	−
Caco-2	−	+	−	−	−	−	−	+	−	+	−
Cardinogenicity (binary)	−	−	−	−	−	−	−	−	−	−	−
Cardinogenicity (trinary)	−	−	−	−	−	−	−	−	−	−	−
Eye irritation	−	−	−	−	+	−	−	+	−	−	−
Fish aquatic toxicity	+	+	+	+	+	+	+	+	+	+	+
Human oral bioavailability	−	+	−	+	+	+	−	+	−	+	+
Acute Oral Toxicity	2.4622	3.2863	3.52675	2.84640	2.7836	2.5094	2.6122	2.7668	3.3177	3.42946	1.9842

Table 4. The compounds with the highest affinity are represented with its 2D image and docking score, formula and SANCDB ID.

S. No.	SANCDB ID	Name of the Compound	2D Image	Formula	Docking Score
1.	SANC00369	Parviflorone F		C27H30O6	−6.9
2.	SANC00265	Tingenine B		C28H36O4	−6.7
3.	SANC00290	Clionamine D		C24H35NO4	−6.6
4.	SANC00342	Kraussianone 1		C25H22O6	−6.6
5.	SANC00347	Kraussianone 4		C25H22O7	−6.6
6.	SANC00352	Kraussianone 6		C25H24O7	−6.6
7.	SANC00436	Mamegakinone		C22H14O6	−6.6
8.	SANC00747	7-Dehydroagapanthagenin		C18H23NO5	−6.6
9.	SANC00257	20-hydroxy-20-epi-tingenone		C28H36O4	−6.5
10.	SANC00413	Bromotopsentin		C20H13BrN4O2	−6.5
11.	SANC00734	Valdivone B		C28H34O5	−6.5

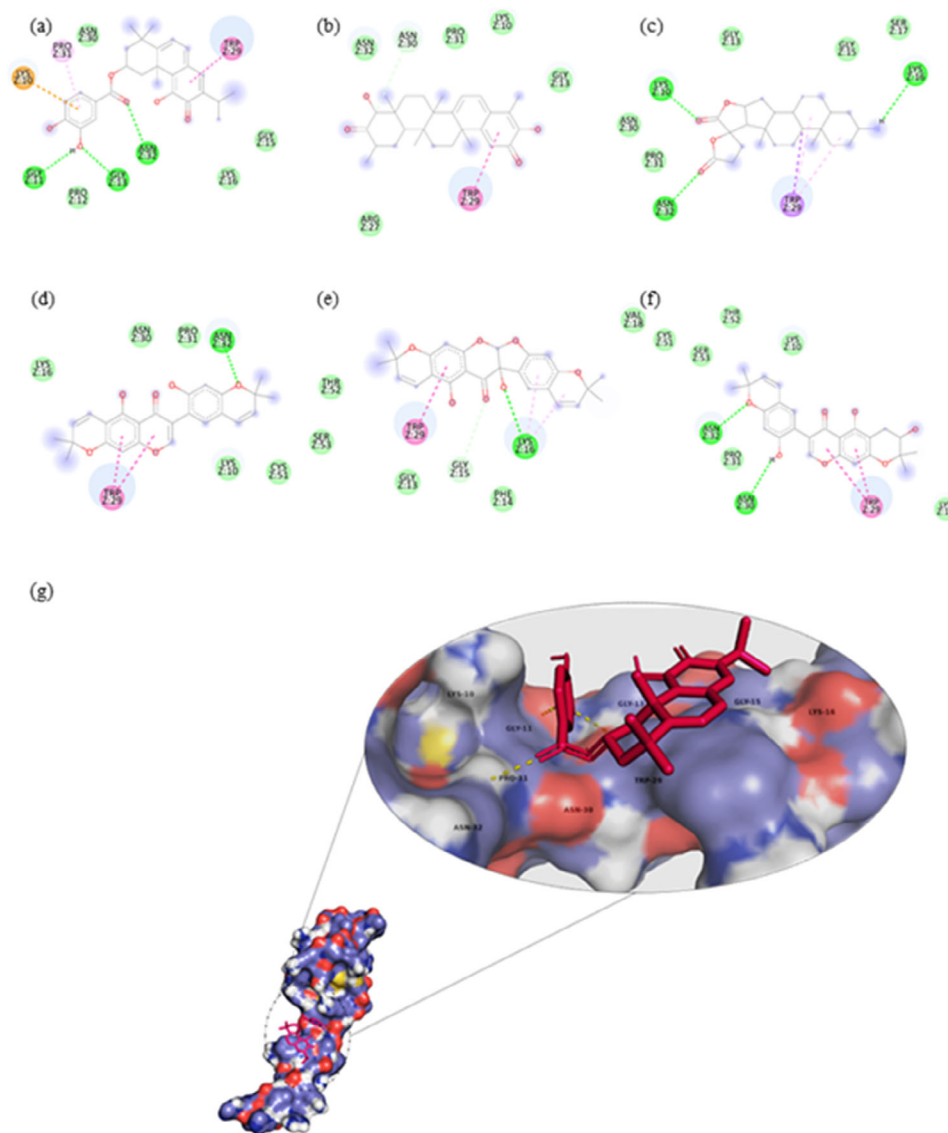


Figure 5. 2D representation of the compounds, parviflorone F (a), tingenine B (b), clonamine D (c), kraussianone 1 (d), kraussianone 4 (e), and kraussianone 6 (f) with the interacting residues of the protein. 3D surface interaction diagram of the protein and the ligand parviflorone F (g).

Madurella mycetomatis, another known causative agent for Mycetoma, which is the only approach that has any hope for vaccine development for the disease. However, researchers have not paid sufficient attention to mycetoma formation induced by *N. brasiliensis*.

AMDET, drug-likeness, and toxicity screening of the compounds yielded 229 compounds with desired properties. Molecular docking further revealed the most effective compounds against the target protein, and the combination of VS and molecular docking resulted in the discovery of potential antimycetoma activity of parviflorone F. This was confirmed by a 100 ns molecular dynamics study, which described the stability of the compound upon binding to the target protein. This study thus revealed the drug-like properties of the compound, while previously, the compound was exclusively studied for its antimalarial activities, and more importantly, its anti-plasmodial activity.^[38] This compound has also been reported to be feasi-

ble as an abietanedi-terpene and can be extracted from various sources, such as plant leaves. *Plectranthus* species belonging to the family Lamiaceae have discovered wide applications in conventional African medication, for instance, in the treatment of gastrointestinal issues, as hostile to microbial agents,^[39] which is one of the major sources of this drug-like compound. Hence, the in silico strategies used in this study indicated that parviflorone F is effective as an antimycetoma compound that acts against the causative agent, *N. brasiliensis*, and possesses active drug-like properties. However, detailed in vitro and in vivo studies would provide further insights into the antimycetoma activity.

5. Conclusions

Nocardia brasiliensis, a major causative agent, requires long-term antibiotic treatment, which is often toxic and expensive.

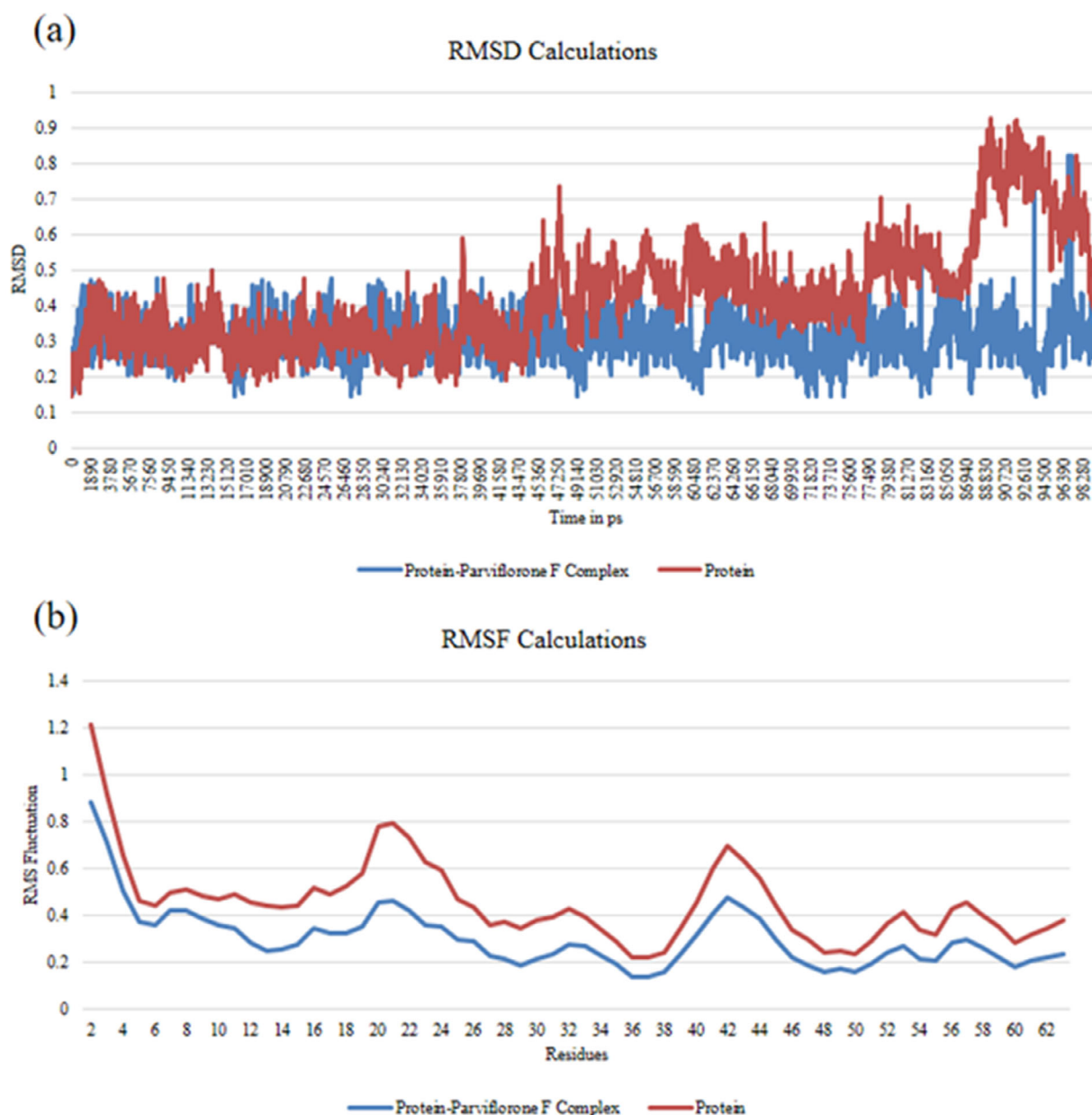


Figure 6. (a) The representation of the protein RMSD as a function of time and (b) RMSF plots of backbone residues and comparison to stability obtained upon the binding of the ligand.

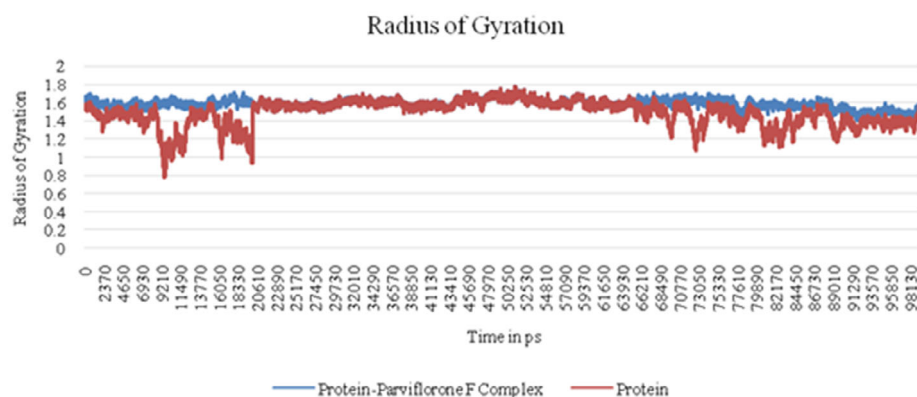


Figure 7. Time evolution of gyration radius (g). The values were presented on a 100 ns MD simulations time scale for the apo protein and protein-parviflorone F complex, which stabilizes the protein structure.

Plant-derived compounds offer a promising alternative with potentially lower toxicity and lower costs. In silico screening was used to identify phytochemicals such as terpenoids (e.g., parviflorone F from *Plectranthus ecklonii*), which are non-toxic molecules that can inhibit *N. brasiliensis* by binding to the 50S ribosomal unit L28 protein. This research helped us in the discovery of a potential molecule with a binding energy of -6.9 Kcal/mol which was relatively higher than that of the control drug amikacin (-4.6 Kcal/mol). The compound follows the Lipinski, Veber, Ghose, Veber, Egan, and Muegge rules, and 55% bioavailability has been reported. MD simulations showed promising results for parviflorone F. This indicated that the compound was efficient in protein inhibition and translation. ADMET screening ensures drug likeness and bioavailability, making it a viable candidate. This study provides new insights into the use of natural products for the treatment of mycetoma. However, future studies should focus on in vitro and in vivo validation to confirm the efficacy of the compound before clinical trials.

Author Contributions

Sowmya Hari and Sandra Jose conceptualized the work. Meenambiga Setti Sudharsan, Manjunathan Jagadeesan, Pasiyappazham Ramasamy, and Shyamala Gowri designed and wrote the manuscript's initial draft. Muthu Thiruvengadam and Baskar Venkidasamy prepared the figures and tables and edited and revised the manuscript critically. The final manuscript has been approved by all authors.

Acknowledgements

This paper was supported by the KU Research Professor Program of Konkuk University, Seoul, South Korea.

Conflict of Interests

The authors declare no conflict of interest.

Data Availability Statement

The data that support the findings of this study are available from the corresponding author upon reasonable request.

Keywords: ADMET · Molecular dynamic simulation · Mycetoma · Neglected disease · *Nocardia brasiliensis* · Parviflorone F

- [1] O. Welsh, H. M. Al-Abdely, M. C. Salinas-Carmona, A. H. Fahal, *PLoS Negl. Trop. Dis.* **2014**, *8*, e3218.
- [2] D. Emery, D. W. Denning, *PLoS Negl. Trop. Dis.* **2020**, *14*, e0008397.
- [3] M. Garnica, M. Nucci, F. Queiroz-Telles, *Curr. Opin. Infect. Dis.* **2009**, *22*, 559–563.

- [4] A. O. Ahmed, W. van Leeuwen, A. Fahal, W. van de Sande, H. Verbrugh, A. van Belkum, *Lancet Infect. Dis.* **2004**, *4*, 566–574.
- [5] W. van de Sande, A. Fahal, S. A. Ahmed, J. A. Serrano, A. Bonifaz, E. Zijlstra, *Med. Mycol.* **2018**, *56*, S153–S164.
- [6] M. E. Brandt, D. W. Warnock, *J. Chemother.* **2003**, *15*, 36–47.
- [7] P. D. Wortman, *Arch. Dermatol.* **1993**, *129*, 564.
- [8] J. T. Carlisle, D. L. Greer, N. E. Hyslop, *J. Infect. Dis.* **1988**, *158*, 244–246.
- [9] A. J. Salter, *Rev. Infect. Dis.* **1982**, *4*, 196–236.
- [10] T. Ogawa, K. Kasahara, S. Yonekawa, C. Nakagawa, K. Maeda, M. Konishi, K. Mikasa, K. Kikuchi, *J. Infect. Chemother.* **2011**, *17*, 706–709.
- [11] V. Berk, W. Zhang, R. D. Pai, J. H. Cate, *Proc. Natl. Acad. Sci. U.S.A.* **2006**, *103*, 15830–15834.
- [12] M. A. Borovinskaya, S. Shoji, K. Fredrick, J. H. Cate, *RNA* **2008**, *14*, 1590–1599.
- [13] C. Ma, D. Kurita, N. Li, Y. Chen, H. Himeno, N. Gao, *Nature* **2017**, *541*, 550–553.
- [14] N. R. James, A. Brown, Y. Gordiyenko, V. Ramakrishnan, *Science* **2016**, *354*, 1437–1440.
- [15] J. S. Lee, G. An, J. D. Friesen, K. Isono, *Mol. Gen. Genet.* **1981**, *184*, 218–223.
- [16] S. E. Motika, P. J. Hergenrother, *Nat. Prod. Rep.* **2020**, *37*, 1395–1403.
- [17] M. H. Medema, *Nat. Prod. Rep.* **2021**, *38*, 301–306.
- [18] D. Szklarczyk, A. L. Gable, D. Lyon, A. Junge, S. Wyder, J. Huerta-Cepas, M. Simonovic, N. T. Doncheva, J. H. Morris, P. Bork, L. J. Jensen, *Nucleic Acids Res.* **2019**, *47*, D607–D613.
- [19] A. Waterhouse, M. Bertoni, S. Bienert, G. Studer, G. Tauriello, R. Gummienny, F. T. Heer, T. A. P. de Beer, C. Rempfer, L. Bordoli, R. Lepore, *Nucleic Acids Res.* **2018**, *46*, W296–W303.
- [20] E. Gasteiger, C. Hoogland, A. Gattiker, M. R. Wilkins, R. D. Appel, A. Bairoch, *Proteomics Protocols Handbook* **2005**, 571–607.
- [21] R. Hatherley, D. K. Brown, T. M. Musyoka, D. L. Penkler, N. Faya, K. A. Lobb, Ö. T. Bishop, *J. Cheminform.* **2015**, *7*, 1–9.
- [22] C. A. Lipinski, F. Lombardo, B. W. Dominy, P. J. Feeney, *Adv. Drug Delivery Rev.* **1997**, *23*, 3–25.
- [23] A. K. Ghose, V. N. Viswanadhan, J. J. Wendoloski, *J. Comb. Chem.* **1999**, *1*, 55–68.
- [24] D. F. Veber, S. R. Johnson, H. Y. Cheng, B. R. Smith, K. W. Ward, K. D. Kopple, *J. Med. Chem.* **2002**, *45*, 2615–2623.
- [25] W. J. Egan, K. M. Merz, J. J. Baldwin, *J. Med. Chem.* **2000**, *43*, 3867–3877.
- [26] I. Muegge, S. L. Heald, D. Brittelli, *J. Med. Chem.* **2001**, *44*, 1841–1846.
- [27] A. Daina, O. Michielin, V. Zoete, *Sci. Rep.* **2017**, *7*, 1–13.
- [28] D. B. Kitchen, H. Decornez, J. R. Furr, J. Bajorath, *Nat. Rev. Drug Discovery* **2004**, *3*, 935–949.
- [29] S. Cosconati, S. Forli, A. L. Perryman, R. Harris, D. S. Goodsell, A. J. Olson, *Expert Opin. Drug Discov.* **2010**, *5*, 597–607.
- [30] J. D. Durrant, J. A. McCammon, *BMC Biol.* **2011**, *9*, 1–9.
- [31] I. Kufareva, R. Abagyan, in *Homology Modeling* (Eds: A. J. W. Orry, R. Abagyan), Humana Press, Totowa, New Jersey **2011**, pp. 231–257.
- [32] M. Y. Lobanov, N. S. Bogatyreva, O. V. Galzitskaya, *Mol. Biol.* **2008**, *42*, 623–628.
- [33] V. Relhan, K. Mahajan, P. Agarwal, P. V. K. Garg, *Indian J. Dermatol.* **2017**, *62*, 332.
- [34] J. A. Stephens, Ph.D. Thesis, University of Cape Town **1987**.
- [35] M. Ramos-e-Silva, R. S. Lopes, B. M. Trope, *Clin. Dermatol.* **2020**, *38*, 152–159.
- [36] C. M. S. Reis, E. G. D. M. Reis-Filho, *An. Bras. Dermatol.* **2018**, *93*, 8–18.
- [37] A. A. Mohammed, A. M. AlNaby, S. M. Sabeel, F. M. Abdelmarouf, A. I. Dirar, M. M. Ali, M. A. Khandgawi, A. M. Yousif, E. M. Abdulgadir, M. A. Sabahalkhair, A. E. Abbas, *Bioinform. Biol. Insights* **2018**, *12*, 1177932218809703.
- [38] R. L. Van Zyl, F. Khan, F. T. J. Edwards, S. E. Drewes, *S. Afr. J. Sci.* **2008**, *104*, 62–64.
- [39] S. B. Babiaka, F. Ntie-Kang, L. L. Lifongo, B. Ndingkokhar, J. A. Mbah, J. N. Yong, *RSC Adv.* **2015**, *5*, 43242–43267.

Manuscript received: September 12, 2024